A MORPHOLOGICAL METHODOLOGY FOR THREE-DIMENSIONAL HUMAN FACE SOFT-TISSUE LANDMARKS EXTRACTION: A PRELIMINARY STUDY

(Article begins on next page)

10 January 2025

A MORPHOLOGICAL METHODOLOGY FOR THREE-DIMENSIONAL HUMAN FACE SOFT-TISSUE LANDMARKS EXTRACTION: A PRELIMINARY STUDY

F. Calignano, E. Vezzetti

Dipartimento di Sistemi di Produzione Ed Economia dell'Azienda, Politecnico di Torino,
Corso Duca degli Abruzzi 24, 10129,Torino, Italy
Tel.: +39 011 5647294; Fax: +39 011 5647299; e-mail: enrico.vezzetti@polito.it

Abstract

Soft tissues facial assessment could be implemented only involving anatomical landmarks. These points are so significant in the medical context because are able to provide significant information about human face morphology and dimensions. At present their detection and location is made by expert physicians with palpation operations. Even if this procedure normally provide reliable information, these results goodness is anyway proportional to the expertise of the physician. Considering that at present many physicians are approaching 3D scanners, that provides human face three-dimensional data, it is possible to implement a robust and repeatable methodology for supporting the physician diagnosis. In order to reach this aim it is necessary to implement a methodology, based on landmarks geometrical codification, that mathematically formalizes the physician visual and palpation analysis on the real patient.

Keywords: Human Face, Soft Tissues Landmarks, 3D Scanners, Automatic Detection

1.0 Introduction

Both craniofacial soft and the hard tissues are important for orthodontic diagnosis. A conventional orthodontic assessment gives greater emphasis to the hard tissues than the soft tissues. This was justified by the fact that an orthodontist operates on teeth, which are included in hard tissues, and cephalograms, one of the most common diagnostic tool, show hard tissues better than the soft ones. However a complete assessment should not be limited to the hard tissue relationships but should also consider the contribution of the patient's soft-tissues.

At present technology improvements have provided three-dimensional non-invasive digitizers, usable directly on human subjects, able to supply the soft tissues morphological data. Unfortunately these tools are only employed experimentally because of the lack of reliable and efficient working protocols able to provide morphological data more useful than those reachable with the conventional approaches. At present in fact the facial anthropometric measures are extracted on patients locating manually on the face a series of physical markers, attached over specific anthropometric points (landmarks), by the physician. Using traditional callipers or more innovative digital image approaches medical information have been normally extracted, even if their reliability depends strongly on the physician ability, because landmarks are correlated with relatively large and curved areas, rather than a discrete point, asking a consistent landmarks knowledge [1].

Working with three-dimensional non-invasive digitizers it is necessary to identify a procedure able to simulate the manual ability of the physician in locating the specific point by palpating or computing the same reference point on bony prominence.

Looking at technical literature some semi-automatic methods for landmark identification with interactive control are described, even if they suffer from a significant

number of false detections [2]. Several studies have been reported on interactive localization of landmarks on dry bone models, laser digitized data [3,4] or medical images [5]. Starting from one of the most known technical paper [6] it is possible to find a comprehensive list of bony landmarks. In this work it is also possible to find the locating procedure description on a patient by palpation. Another research work [7] carried out experimental studies on manual location of lower limb landmarks on dry bone models with a group of surgeons and concluded that the variations are in the range 6–25mm. It is possible to find a manually identification procedure [3] for a scanned surface of foot model, guided by curvature values, for evaluating tibial torsion. Reproducibility of the results appears to be dependent on user's knowledge of landmarks. The effect of scanning artefacts is not very clear. Other researchers [8] studied the relationships between bony and soft tissue landmarks using cephalometric radiographs to diagnose facial growth abnormalities prior to treatment. Working at the same with a manual procedure [9] a new methodology has been proposed for extracting anatomical landmarks on a 3D model reconstructed from MRI images for morphometric analysis. A method that classifies each point on both the pre- and post-operative facial surfaces into one of eight types of surface patch have been developed [10]. This classification is based on the mean and Gaussian curvatures of the surface around each point. Adjacent points with the same classification are grouped into surface patches. This method has the potential to supply shape change information, but unfortunately no algorithm has been developed for automatically calculating correspondence between patches.

Together with these just cited method the technical literature proposes also some works in landmarks repeatability but no one is focused on the development of a methodology for supporting a formal codification of soft-tissues landmarks and consequently their automatic extraction from a point cloud. For this reason next paragraphs will deal with a procedure for managing a points cloud with the aim of identifying soft-tissues landmarks.

1.1 Pathology and Landmarks

The selected facial pathology was the malocclusion, characterized by the misalignment between the upper and lower mandibular structures (Figure 1), which is treated with a surgical translation of the mandible. This study was undertaken on twenty-one Caucasian adult, treated with bilateral sagittal split osteotomy surgery (BSSO) [11], divided into eleven males and ten females, that have been digitised before and after the surgery with a 3D laser scanner *Cyberware Scanner 3030RGB* (Cyberware Laboratories, Inc., Monterey, California). This sample consisted of patients who were diagnosed with mandibular prognathism (12 patients) and mandibular retrognathia (9 patients). Five patients show also facial and nose asymmetry.
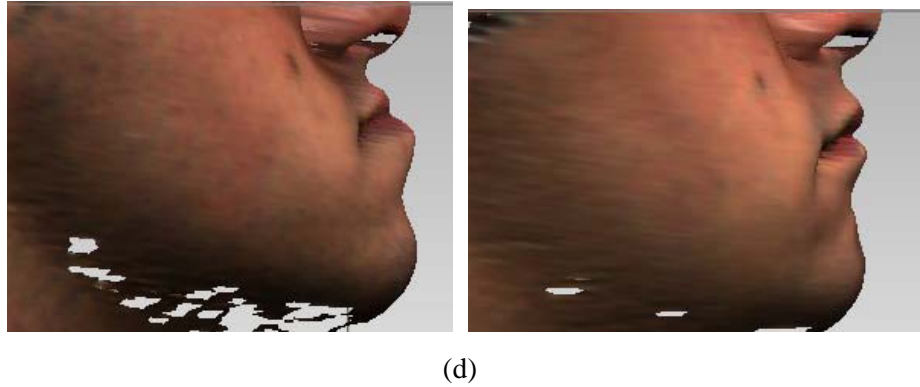

(a)　　　　　　　(b)　　　　　　　(c)

(d)
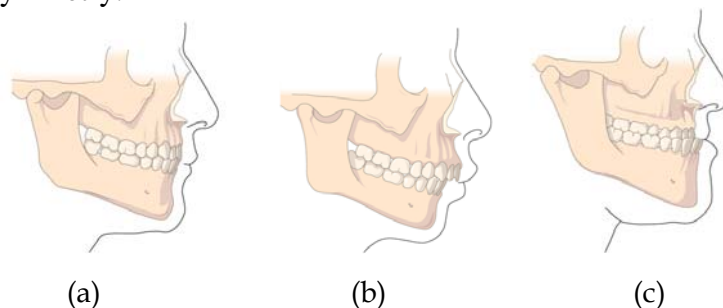
Figure 1. Schematic example of malocclusion: (a) Class I,Orthognathic (b) Class II,Retrognathic (c) Class III,Prognathic, (d) one example of the case studies (pre and post surgery).

One way to achieve correspondences between the different shapes is to use landmarks that are manually placed on 3D features of the face. The landmarks should be placed on anatomically distinct points of the face in order to ensure proper correspondence. However, parts of the face such as the cheeks are difficult to landmark because there are no uniquely distinguishable anatomical points across all faces. It is important to choose landmarks that contain both local feature information (eg. the size of the mouth and nose) as well as the overall size of the face (eg. the location of the eyebrows). Previous work on 3D face modelling for classification has shown that there is not much difference between the use of 11 and 59 landmarks [12].

For each patient the three-dimensional coordinates of the 16 facial soft tissue landmarks (Figure 2) have been identified on point cloud.

Name	Abb.
Nasion	*n*
Pronasale	*prn*
Subnasale	*sn*
Labiale superius	*ls*
Sublabiale	*sli*
Pogonion	*pog*
Nasal alar crest	al_{right}, al_{left}
Cheilion	ch_{right}, ch_{left}
Endocanthion	en_{right}, en_{left}
Exocanthion	ex_{right}, ex_{left}
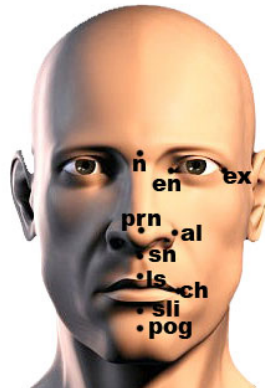
Figure 2. Soft tissues morpohological reference points (landmarks).

2.0 Landmarks extraction: the proposed methodology

Many applications, such as deformation analysis, animation and face recognition, involves the accurate identification of feature points (landmarks) on external body parts working on points clouds. Landmarks points identification could be decomposed in two steps: *detection* and *localization* [13].

In the human face landmarks identification this split involves a refining process that at the beginning detects the interesting areas, around those areas on the face where the physician know the landmark is located

Next step, the localisation procedure, in order to provide more detailed information about the already area identified it is necessary to analyse the shape changes localising from a morphological point of view and than, going ahead with more detail,

Landmark detection is used for relating vertices from different scans (prior to registration), for generating signatures (for biometrics) and for segmenting regions of interest. Most existing methods for landmark detection on meshes are dependent on prior knowledge of feature map thresholds, orientation and pose [14,15]. Deformable models such as Active Shape Models (ASM), Active Appearance Models (AAM) and 3D Morphable Models (3DMM) are extensively used for image segmentation and landmark detection [16,17]. The shape model used in these approaches, called Point Distribution Model (PDM), aims to perform image interpretation using prior statistical knowledge of the shape to be found. In AAMs texture information is also modelled and associated with the corresponding point locations for model fitting. 3DMM is a concept closely related to AAMs where a 3D model is used to estimate the 3D parameters in a 2D image and to segment objects [18,17]. Recently the PDM was adapted for 3D volumetric data [19] and reconstruction of 3D meshes [20]. Some algorithms attempt to extract features/regions of the face based on the shape of the face and classify these regions based upon the results. These approaches uses differential geometry [21,22]. Some approaches [23] have been used for refining the estimated position from 3D differential operators, and thus allow improved localization of the landmark. It has been performed an evaluation study focusing on the detection performance of nine different 3D differential operators [24].

Moving the attention on location some methods involve surface curvature analysis [25-27]. Effectively, an efficient way to automate the procedure, increasing robustness and repeatability, and reduce false identifications in the landmarks automatic extraction could be based on their invariant geometric characteristics, as curvatures. Surface curvature, independent from patients position and orientation, can support the detection of such geometrical features. A set of common geometric shapes such as *peak*, *ridge*, *pit*, and *ravine* is observed in regard to the anatomical landmarks on hard and soft tissue in the approaches based on curvature surface (Figure 3). A *peak* can be described as a point with local maximum real-valued function and high gradient with respect to surroundings. A *ridge* is a narrow, raised strip of line formed at the junction of two sloping surfaces diverging towards the ground. In its broadest sense, the notion of peak and ridge generalizes the idea of a local maximum of a real-valued function such as curvature and its derivatives. *Pit* and *ravine* have a similar characteristic that is they represent a local minimum of an intrinsic real-valued function. Pit is a point surrounded by a high walled locally depressed region on surface. A ravine can be defined as a line formed by intersection of two concave surfaces.
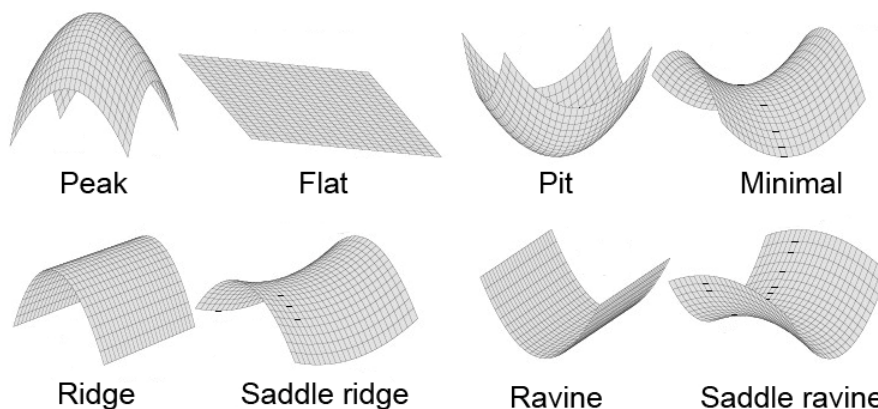

Figure 3. Geometric shape

The curvature, therefore, allows to locate the anatomical landmarks that are points or distinct regions on soft tissue with uniqueness in shape characteristics in their vicinity, and these regions can be classified on the basis of their shape characteristics. The curvature permits to segment the face into regions, based on its homogeneity in specific characteristic, for recognition or to locate feature points for registration and analysis on pre and post surgery.
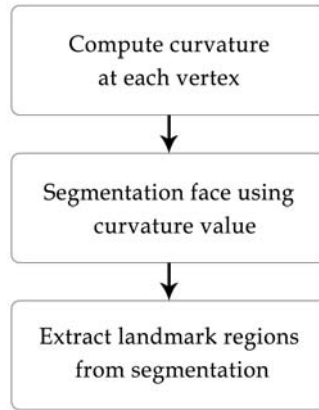

Figure 4. Overview of the methodology for identifying landmarks.

2.1 Compute curvature at each vertex.

Several techniques have been developed to estimate the curvature information in the last decade. From the mathematical viewpoint, the curvature information can be retrieved by the first and second partial derivatives of the local surface, the local surface normal or the tensor voting. From the computational viewpoint, there are analytic and numerical methods. As to the input data type, the curvature information can be estimated from the range data, the intensity data or 3D sparse data. FLYNN and JAIN [28] evaluated five curvature estimation methods and classified them into two categories: analytic methods [29, 30] and numerical methods [31,32]. Analytic methods fit a surface to range values in a local patch and determine the curvature information using the first and the second partial derivatives computed from the surface equation. Analytical methods differ in their local surface fitting algorithms. Numerical methods do not fit a surface, but estimate the curvature or the derivatives of the surface numerically, as done in the surface normal change methods and the directional curvature methods. Similarly, SHI et al. [33] also estimated the surface normal. TANG and MEDIONI [34] presented a novel approach based on the concept of "tensor voting" to recover the curvature information. Both the sign and the direction of principal curvatures are inferred directly from the input, which can be 3D sparse data. Since their approach does not demand local surface fitting, it can be viewed as a numerical method as well. Even with extensive research on curvature estimation in the past, it is still difficult to generate satisfactory results in all cases. It was observed empirically [29, 35] that qualitative curvature properties can be more reliably estimated than quantitative ones. Thus, some research efforts only focus on the recovery of the sign of the Gaussian curvature instead of its magnitude. ANGELOPOULOU and WOLFF [36] computed the sign of the Gaussian curvature by checking whether the relative orientation of two local closed curves (one from the surface and the other from its corresponding curve on the Gauss sphere) is preserving or reversing. An alternative curvature representation [37] is based on the parameterization of the structure in two features maps, namely the *shape index, S,* and the *curvedness index, C*. These index (*S*, *C*) can be viewed as polar coordinates in the (k_1, k_2) – plane (Figure 5), with planar points mapped to the origin.
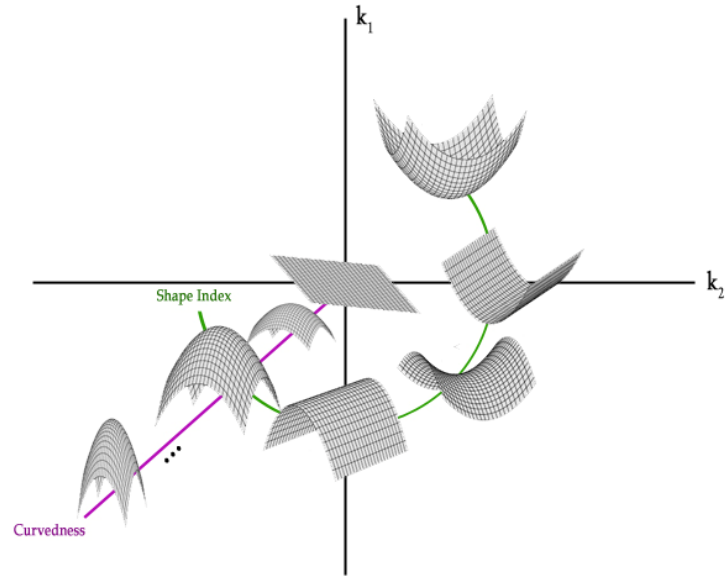
Figure 5. The effects on surface structure from variations in the Curvedness (radial coordinate) and Shape Index (angular coordinate) parameters of curvature, and the relation of these components to the principal curvatures (k_1 and k_2). The degree of curvature increases radially from the centre.

Therefore, these indices, S and C, well analyze human face when these data comes from as cylindrical acquisition as the major part of the medical acquisition devices (MRI, TAC, 3DScanner Cyberware, etc).

Like the Gaussian and mean curvature, these features maps can be defined through the *principal curvature*, k_1 and k_2 , that measure how the surface bends by different amounts in different directions at that point (Appendix A1). The Shape Index is invariant over arbitrary scaling transformations. Thus, a point on a large sphere would have a different Curvedness than would a point on a small sphere, but they would both have the same Shape Index. The variations of 3D surface structure as a function of these parameters is illustrated graphically in figure 6. Local shape varies around the origin from convex spherical through cylindrical and saddle-shaped to concave spherical (Figure 6 and 7). Given, e.g. two convex parabolic points, that are identical under the shape index descriptor, they may be more or less 'curved' and/or oriented differently. This is the overall magnitude of curvature and it is determined by the Curvedness parameter (Figure 6).
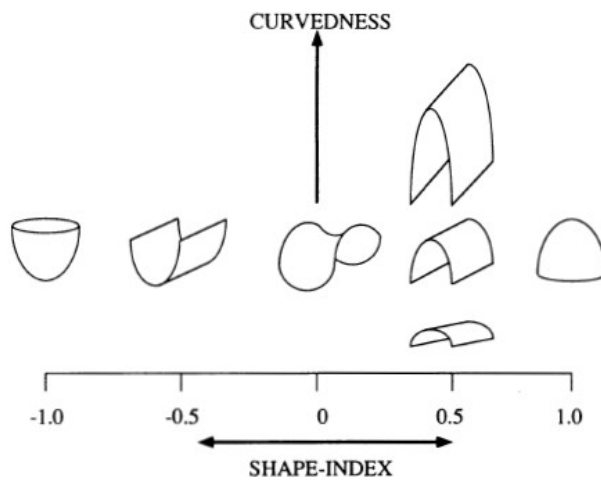
Figure 6. Shape index and Curvedness
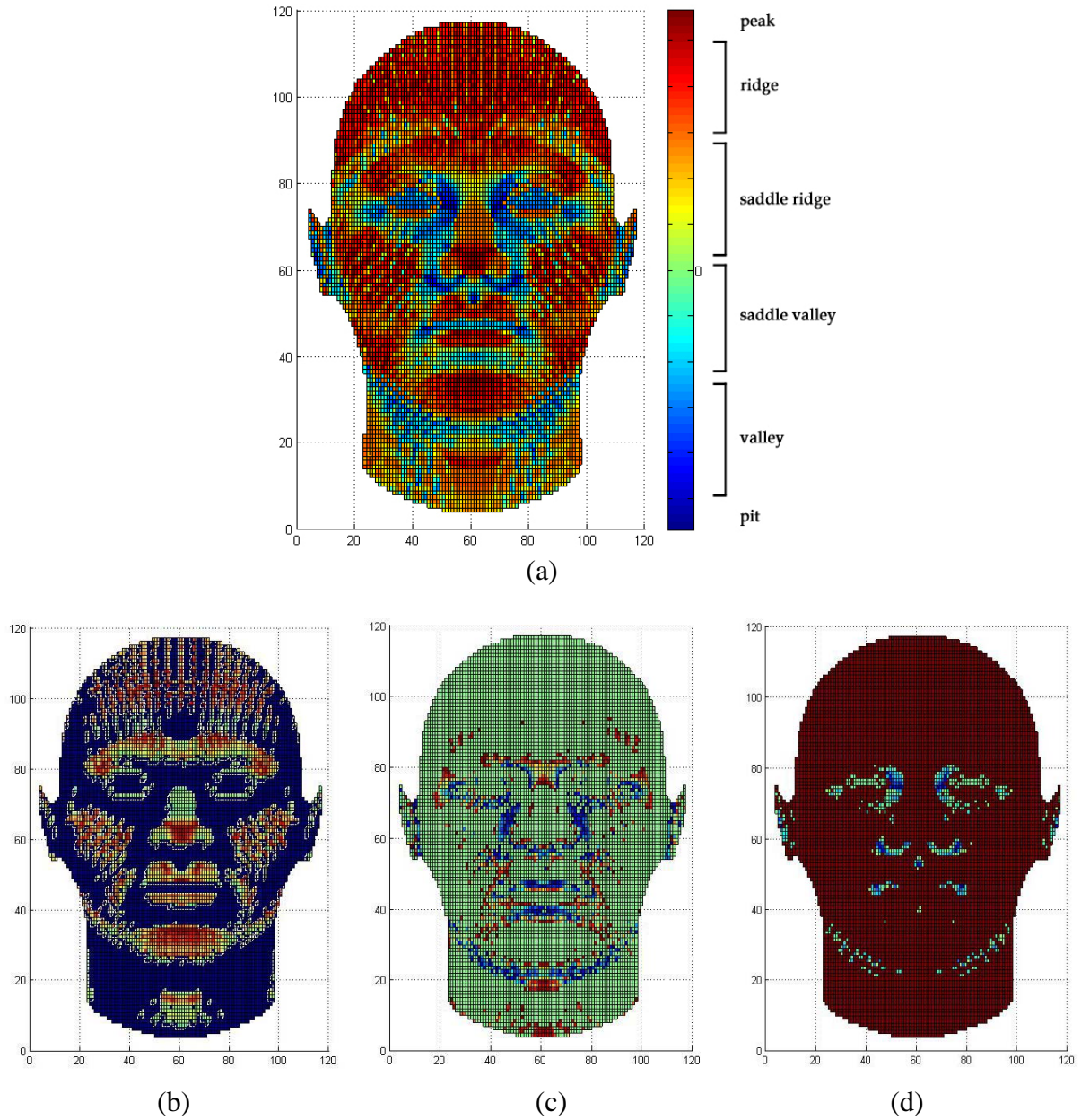
Figure 7. (a) Shape Index on mean human face;(b) Saddle ridge, (c) Minimal, (d) Saddle valley.

Class	H	K	Type	S
Peak	-	+	Elliptical concave	[0.625, 1)
Ridge	-	0	Cylindrical concave	[0.375, 0.625)
Saddle ridge	-	-	Hyperbolic concave	[0.125, 0.375)
Plane	0	0	Planar	
Minimal	0	-	Hyperbolic symmetric	[-0.125, 0.125)
Pit	+	+	Elliptical convex	[-0.625, -1)
Valley	+	0	Cylindrical convex	[-0.625, -0.375)
Saddle valley	+	-	Hyperbolic convex	[-0.375, -0.125)

Table 1. Topographic classes.

2.2 Segmentation face using curvature value

For landmark localisation many methods first segment part of the structure in a neighbourhood of the landmark, and then localize the landmark by analyzing the segmented part. Segmentation is the process which provides the necessary organization of the data points by partitioning them into connected regions or parts that can be approximated by standard surfaces (e.g. planes, cylinders, etc.) or volumetric primitives (e.g. super-ellipsoids). The quality of segmentation is a crucial issue that is directly related to the corresponding application which imposes particular requirements. There is a variety of algorithms for 3D mesh segmentation (Appendix A2), which can be grouped in two basic categories: *surface-based*, the 3D mesh is segmented into regions which represent distinct surfaces of the model and can be approximated by various primitives like planes, cylinders, spheres, polynomials, etc; *part-based*, the 3D mesh is segmented into volumetric parts which can be approximated by volumetric primitives (e.g. super-ellipsoids). For *surface-based algorithms* it is usually required that the boundaries of the segmented regions should be smooth, the extracted regions should be able to be approximated by smooth surfaces, and the boundaries where the regions meet should allow certain types of continuity to hold for the approximating surfaces. For *part-based algorithms* a variety of criteria can be used in order to be able to extract the meaningful parts of the object. The most used criterion is the minima rule introduced by HOFFMAN and RICHARDS [38] which states that an object is segmented by human perception at areas of concavity. This criterion has been adopted by many researchers [39-47] to segment 3D meshes. The quality of segmentation is also directly dependent on the type of the object that is being processed.

The surface segmentation method presented in this paper is based on morphological watersheds, which are used in image processing to achieve sensible, reliable partitioning of images. For images the algorithm commonly operates on the gradient magnitude of the input image. For 3D surface meshes, it uses the curvature of each vertex on the surface.

The watershed segmentation algorithm consists of two steps. The first step is the identification of distinct catchment basins (Appendix A2, figure A2.1). The second step is a region merging process, which combines insignificant regions identified by the depth of the catchment basin, thereby making the results less sensitive to noise.

The steps of the watershed segmentation algorithm are summarized as follows:

- *Input*: Smoothly triangulated 3-D surface model.
- *Step 1*. Compute Shape Index and Curvedness for each vertex on the surface.
- *Step 2*. Locate all local minima, each of which forms the bottom of a catchment basin.
- *Step 3*. Flat regions with uniform curvature are then found and classified depending on whether they have any neighboring vertices adjacent to their boundaries lower than their curvature or not.
- *Step 4*. Merge shallow regions with their neighbors until the depths of all remaining regions are above a preset threshold.

The input to the watershed method is a surface mesh and whatever additional information (e.g., surface normals) is necessary to calculate the curvature at each vertex. For tessellated surfaces, the model is frequently sparse, with just enough vertices to define each surface (particularly a problem in planar areas), and some large regions might not contain enough vertices to define a catchment basin with an associated boundary. This problem can be solved by creating a new mesh, the dual of the original, which has a node for each edge in the original mesh and a connection to each adjacent edge (now nodes) across the faces of the two neighboring triangles (or polygons). This new mesh is the input of the segmentation algorithm (Figure 8). The algorithm then segments this mesh, using the curvature. Thus, the first step of the segmentation is the calculation of curvature at each vertex on the surface. The method for

calculating curvature should depend on the application and type of input data available. The methods for curvature calculation used in this work are Shape Index and Curvedness. The watershed algorithm is independent of the type of curvature used.

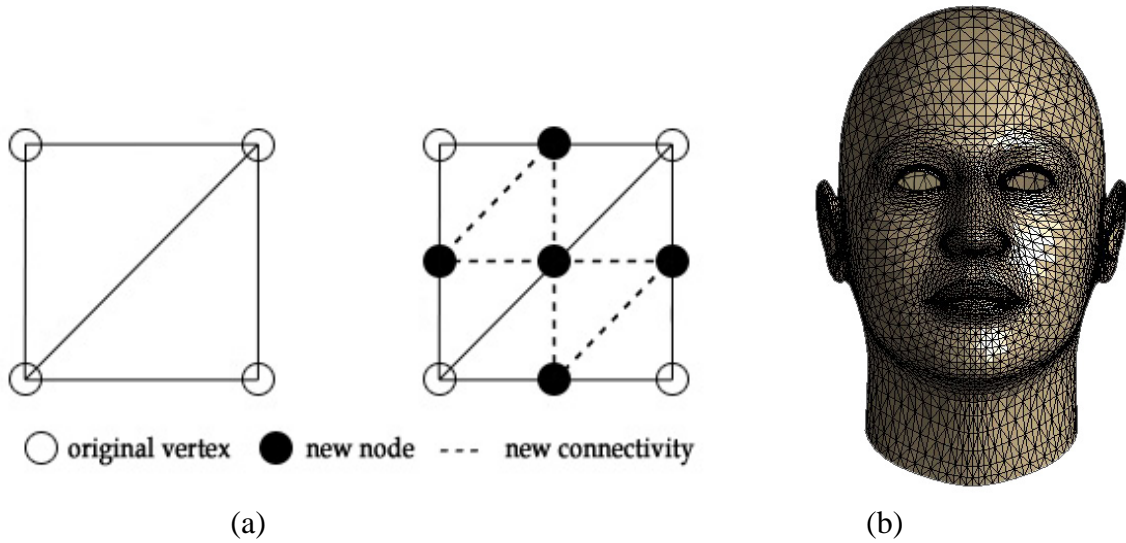(a)   (b)

Figure 8. (a) Creation of edge-based topology based on original mesh; (b) new mesh.

After the computation of the curvature, it is applied a threshold of curvedness, t_C, to the curvature to extract the zones of interest (C> t_C). C varies from zero for a flat surface up to infinity for an extremely curved surface. Each minimum serves as the initial seed for a surface region, i.e. a distinct region on the surface formed during the descent of vertices along their paths of steepest descent (Appendix A2, figure A2.2). Curvature map allows to segment the surface into regions based on its homogeneity in specific characteristic. The t_C value used to is performed so that relatively flat areas where the curvature is extremely low throughout will be classified as flat, easing the computational burden and reducing the noise.

The region merging is done based on the importance of a given region. The depth of the region is used as a measure of the region's significance. There are a variety of possibilities for metrics that indicate insignificant regions, but the watershed algorithm itself gives a fairly reliable metric for determining the valency of a segment. This metric is the greatest depth of water that a segment can hold before it "spills over" into one of its neighbors. Regions that are "shallow" are relatively constant in curvature, i.e., their boundaries have a curvature which is not significantly greater than the flattest part of that region. The watershed depth can be calculated as the difference between the point in the region with the overall lowest curvature (the local minimum) and the vertex along the region's boundary with the lowest curvature of all other boundary vertices (Appendix A2, figure A2.3). This is the depth of water that the region can hold before it begins to overflow its boundary.

After final step, you delete the regions close to those of interest in order to reduce the computational analysis and identification of possible false landmark (Figure 9).
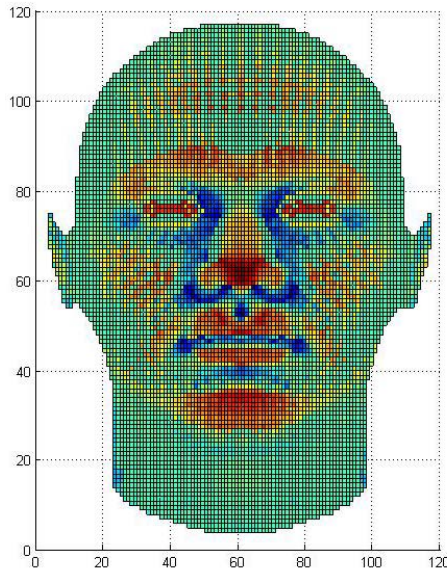
Figure 9. First segmentation: zones of interest with shape index values.

2.3 Extract landmark regions from segmentation

For some individuals, even if the image was considered of good quality, the facial surface was not completely captured, with voids evident in certain areas, particularly around the hairline and nose. Moreover, some landmark, such as *nasion*, is not easily identifiable, especially in female. Using the Shape Index is possible, however, identify the area. In fact, soft tissue *nasion* is defined in the Anthropometry as the point of maximum concavity and maximum convexity on the bridge of the nose and therefore it is located as the point where the local surface most closely approaches the symmetric saddle shape.

The values of the Shape Index can be use to obtained the information on the saddle ridge, minimal and saddle valley zones in the human face (Figure 7). Every distinct shape, except for the plane, corresponds to a unique value of S (table 1).

It was seen that with a threshold value of $t_C = 0.05$ it is possible obtained further segmentation of the human face's regions (Figure 10a) in order to have a most rapid extrapolation of the landmarks.

From figure 10b it can be seen that important facial landmarks like *cheilions* (lip corners), *endocanthion* and *exocanthion* internal and external eye corner, *nasion*, left and right nasal *alae, pronasale*, *pogonion*, *labiale superius* are lateral extremal boundary vertices of detected feature regions and can thus be identified.

Figure 10. (a)Second segmentation - Landmark regions on shape index map with threshold value applied; (b) anatomical landmarks.

3.0 Experimental validation

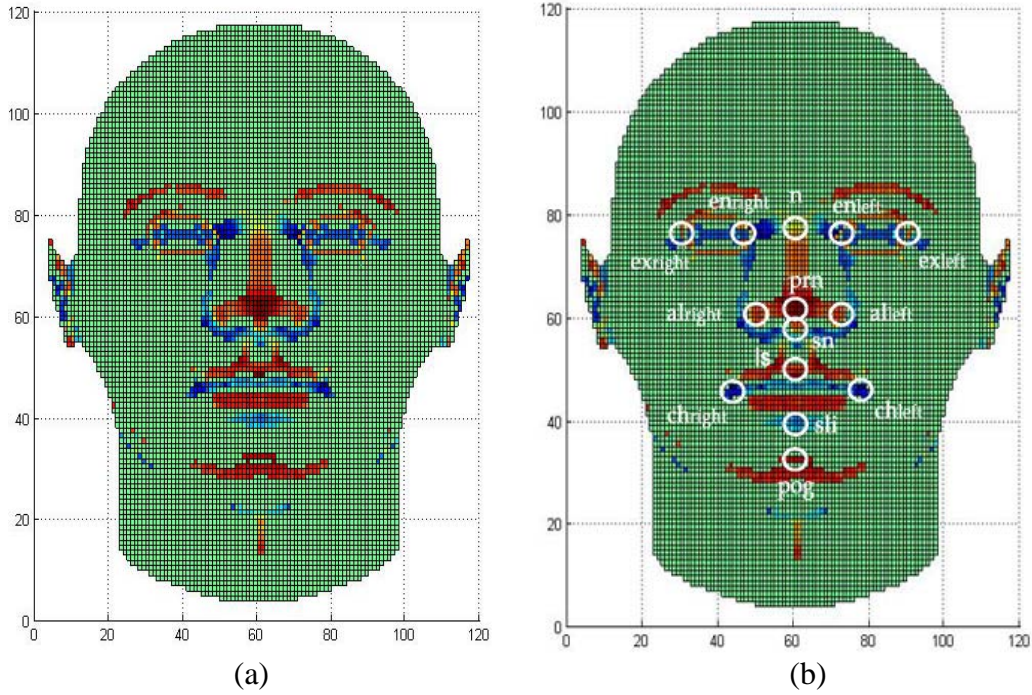In order to evaluate the performance of the proposed methodology, the *x*, *y* and *z* coordinates of the landmarks identified (Figure 10b) have been used to calculate some soft tissue distance: en_{right}-en_{left} (distance between right and left endocanthion), ex_{right}-ex_{left} (distance between right and left exocanthion), $al_{right} - al_{left}$ (nose width), $ch_{right} - ch_{left}$ (mouth width), *sn-prn* (nasal tip protrusion), *sn-pog* (anterior lower facial height). Then these measurements have been compared with the ones obtained using landmark markers pasted of the technician on patient's face. (table 2).

			Distance [mm]					
			ex_r-ex_l	en_r-en_l	$a\ l_r$-al_l	ch_r-ch_l	sn-prn	sn-pog
Face 1	A.L.E.	Pre	92.09	35.87	33.23	47.58	16.63	55.88
		Post	95.59	33.48	34.31	45.91	18.33	55.76
	Marker	Pre	92.97	34.27	33.32	46.21	19.68	55.77
		Post	93.10	34.87	33.39	53.14	17.71	52.15
Face 2	A.L.E.	Pre	94.03	30.85	33.12	44.69	23.99	68.69
		Post	94.92	29.64	35.27	43.74	24.77	53.96
	Marker	Pre	90.00	30.28	34.07	50.74	25.31	65.30
		Post	93.66	29.64	37.34	52.11	22.70	51.67
Face 3	A.L.E.	Pre	96.88	32.10	34.40	55.95	28.92	47.49
		Post	102.31	32.76	35.61	52.61	23.20	54.07
	Marker	Pre	92.94	31.57	33.36	58.29	30.31	45.55
		Post	100.35	33.12	35.78	56.35	25.33	49.42
Face 4	A.L.E.	Pre	89.58	29.97	29.52	41.50	20.66	50.89
		Post	91.89	28.66	32.64	42.05	21.55	44.25
	Marker	Pre	90.78	30.59	29.32	43.18	23.25	44.96
		Post	91.27	30.48	33.44	46.60	20.58	44.44

Face 5	A.L.E.	Pre	103.51	30.77	32.51	41.46	22.77	66.41
		Post	102.23	31.85	35.53	47.96	24.78	60.06
	Marker	Pre	99.08	28.89	32.86	44.28	24.48	62.87
		Post	98.84	32.74	37.41	49.13	24.91	60.45
Face 6	A.L.E.	Pre	99.22	30.73	33.42	42.32	18.11	65.17
		Post	98.92	37.53	37.21	42.31	18.55	61.46
	Marker	Pre	97.24	36.01	34.17	47.08	20.72	54.06
		Post	97.74	39.86	38.44	50.46	17.96	59.18
Face 7	A.L.E.	Pre	94.61	36.02	32.12	43.19	22.34	45.28
		Post	95.10	36.14	31.14	42.69	20.71	45.95
	Marker	Pre	93.79	36.52	32.56	47.89	20.93	46.55
		Post	92.66	37.69	32.84	44.39	21.24	45.15
Face 8	A.L.E.	Pre	104.17	34.42	35.57	49.78	19.80	58.25
		Post	96.81	39.57	40.77	54.35	20.49	54.38
	Marker	Pre	98.21	37.87	36.66	56.55	22.94	53.44
		Post	95.38	40.26	40.94	60.18	19.37	52.70
Face 9	A.L.E.	Pre	100.75	35.21	36.87	50.73	20.89	62.86
		Post	98.72	37.10	38.87	48.60	20.36	58.45
	Marker	Pre	95.93	43.70	37.16	53.87	22.79	61.60
		Post	97.07	37.48	39.77	54.99	21.69	58.31
Face 10	A.L.E.	Pre	94.36	31.65	31.93	48.01	20.34	46.80
		Post	88.09	31.18	32.43	45.33	22.14	42.90
	Marker	Pre	93.07	32.42	31.59	51.18	21.34	44.38
		Post	86.15	27.72	34.78	51.35	22.21	40.39
Face 11	A.L.E.	Pre	91.57	37.47	35.29	42.19	19.75	61.70
		Post	93.18	37.20	37.37	45.48	21.66	54.40
	Marker	Pre	94.57	39.33	37.11	45.84	21.21	56.72
		Post	95.27	42.16	38.67	41.69	20.69	56.44
Face 12	A.L.E.	Pre	86.64	33.01	31.22	40.23	18.78	54.91
		Post	97.50	38.76	36.60	44.35	17.58	52.02
	Marker	Pre	85.15	33.21	31.06	43.62	19.40	53.42
		Post	96.95	37.16	37.39	46.84	17.78	51.94
Face 13	A.L.E.	Pre	82.83	35.03	29.72	39.74	18.99	36.09
		Post	86.48	34.39	31.28	42.13	20.34	37.99
	Marker	Pre	85.58	35.39	30.72	45.50	18.06	34.25
		Post	83.74	34.41	30.78	45.42	20.28	40.89
Face 14	A.L.E.	Pre	92.72	32.44	34.29	44.62	21.20	46.56
		Post	93.49	34.28	39.11	47.90	19.85	47.37
	Marker	Pre	89.76	34.33	34.91	49.52	18.76	46.86
		Post	91.63	35.24	38.52	55.04	19.84	46.22
Face 15	A.L.E.	Pre	89.68	39.29	32.90	47.07	23.53	42.29
		Post	90.91	32.29	28.68	46.62	19.32	48.71
	Marker	Pre	88.54	40.84	32.98	49.67	20.95	46.39
		Post	88.73	38.83	34.54	53.86	18.79	49.30
Face 16	A.L.E.	Pre	82.31	34.76	31.16	40.59	17.79	64.11
		Post	90.69	37.76	39.50	44.78	19.99	61.60
	Marker	Pre	82.98	33.72	30.82	45.47	21.44	63.85
		Post	91.57	40.07	39.45	51.88	22.23	60.21
Face 17	A.L.E.	Pre	88.27	40.35	35.94	46.98	22.36	61.61

|								
		Post	90.49	37.94	35.15	48.46	22.19	58.67
	Marker	*Pre*	85.06	42.20	36.38	54.41	25.71	55.30
		Post	86.22	41.56	35.73	53.29	24.02	56.13
Face 18	*A.L.E.*	*Pre*	90.11	29.91	29.86	47.67	18.23	55.73
		Post	83.87	30.05	29.86	41.83	19.34	49.95
	Marker	*Pre*	84.29	36.37	30.45	50.07	21.47	51.43
		Post	83.03	38.50	31.47	49.16	19.84	48.65
Face 19	*A.L.E.*	*Pre*	89.27	36.56	27.87	33.12	19.06	53.02
		Post	83.65	40.39	28.26	40.21	17.37	54.46
	Marker	*Pre*	83.60	36.56	28.55	45.06	19.16	49.85
		Post	86.13	38.27	30.00	46.91	19.61	53.36
Face 20	*A.L.E.*	*Pre*	93.54	36.82	36.14	47.12	21.69	54.05
		Post	94.49	37.24	38.14	49.04	20.37	55.79
	Marker	*Pre*	91.39	38.68	35.79	47.07	20.95	57.58
		Post	90.73	40.17	36.00	49.06	20.60	55.73
Face 21	*A.L.E.*	*Pre*	87.45	31.76	33.45	46.21	22.66	52.34
		Post	84.16	33.15	34.42	43.00	23.15	49.44
	Marker	*Pre*	85.58	34.78	32.87	46.83	22.58	52.70
		Post	86.95	32.34	34.73	45.26	23.15	48.99

Table 2. Soft tissue measurement.
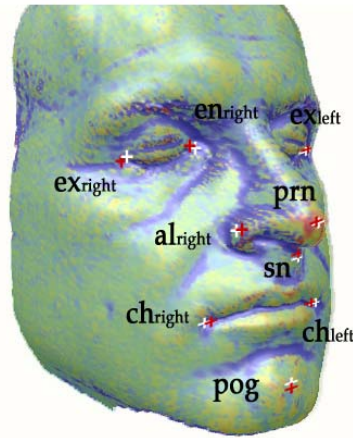
Figure 11. White cross: landmark extracted; Red cross: marker

The mean values and standard deviations of the coordinate values (*x, y, z*) and measurements (Table 3) of each sex were calculated.

			Distance [mm]					
			ex-ex	*en-en*	*al-al*	*ch-ch*	*sn-prn*	*sn-pog*
m_{male}	*A.L.E.*	*Pre*	95.28	34.10	34.06	45.68	21.63	58.92
		Post	96.08	35.62	36.87	47.17	21.50	55.49
	Marker	*Pre*	92.69	35.86	34.55	50.36	23.15	55.64
		Post	94.58	37.26	37.72	51.77	21.82	54.17
m_{female}	*A.L.E.*	*Pre*	89.55	33.99	31.58	43.83	20.06	50.20
		Post	89.66	33.96	32.66	44.05	19.95	49.13

	Marker	*Pre*	88.09	35.31	31.66	46.84	20.69	49.07
		Post	88.68	35.27	33.65	48.76	20.06	48.58
s_{male}	*A.L.E.*	*Pre*	6.59	3.09	1.77	4.74	3.10	8.47
		Post	4.12	3.07	2.71	3.87	2.04	5.26
	Marker	*Pre*	5.25	4.72	2.09	4.78	3.18	7.20
		Post	4.01	4.08	2.27	5.29	2.33	5.50
s_{female}	*A.L.E.*	*Pre*	3.40	3.19	2.44	4.98	2.13	6.55
		Post	5.15	3.80	3.27	2.69	1.93	5.89
	Marker	*Pre*	3.69	3.00	2.13	2.72	1.61	6.84
		Post	4.36	4.07	2.34	3.12	1.74	5.19
s_{male}/m_{male}	*A.L.E.*	*Pre*	0.07	0.09	0.05	0.10	0.14	0.14
		Post	0.04	0.09	0.07	0.08	0.09	0.09
	Marker	*Pre*	0.06	0.13	0.06	0.10	0.14	0.13
		Post	0.04	0.11	0.06	0.10	0.11	0.10
s_{female}/m_{female}	*A.L.E.*	*Pre*	0.04	0.09	0.08	0.11	0.11	0.13
		Post	0.06	0.11	0.10	0.06	0.10	0.12
	Marker	*Pre*	0.04	0.08	0.07	0.06	0.08	0.14
		Post	0.05	0.12	0.07	0.06	0.09	0.11

Table 3. Average (m) and Standard Deviation (s)

Looking at the ratio between standard deviation σ and average value μ, of the two methods, it is possible to see that while for men the proposed method is slightly more stable than the manual, for women the results are exactly the opposite. In order to obtain more information by comparing of the measures obtained with proposal methodology and traditional method, the Normalized Error (E_N) concept [48] was adopted (Table 4, Appendix A3). This is useful for comparisons of measurement results produced at the same hierarchical level, i.e. where no value can be taken as the reference value. In this case, it is necessary to understand whether the difference in the compared results is due to an effective difference between the evaluated properties or to a significant bias between the assessment tools, rather than to random effects.

An E_N value lower or equal than unity indicates that the laboratory value and the reference value agree with each other within their respective uncertainties and is considered a success. An E_N value higher than unity is considered a failure.

Looking at the values obtained, it possible to see only one result outside of the range for female.

		Distance [mm]					
		ex-ex	*en-en*	*al-al*	*ch-ch*	*sn-prn*	*sn-pog*
$E_{N,male}$	*Pre*	0.44	0.44	0.25	0.99	0.49	0.42
	Post	0.37	0.46	0.34	1.00	0.14	0.25
$E_{N,female}$	*Pre*	0.41	0.42	0.03	0.74	0.33	0.17
	Post	0.20	0.33	0.34	1.60	0.06	0.10

Table 4. Normalized Error

4.0 Conclusions

Looking at the results of the experimental validation it is possible to verify the reliability of the proposed method. Moving from diagnostic analysis developed on 2D images to evaluations made on 3D data, as what is possible to obtain working with non invasive 3D

scanners, the passage is significant. While from one side, the availability a 3D morphometric data set could provide a more complete diagnostic support, from the other side the absence of standardised procedures providing a simple management of these 3D points clouds, as they come out from the 3D scanner, represent a big deal. For this reason the availability of a reliable methodology supporting the physician in the interaction with 3D points clouds, and in particular with the anatomical landmarks, could represent the solution to fill this gap. In this way the procedure could simplify the application of those procedures [49] evaluating volumes and areas of the patients facial soft tissues. This methodology could represent the starting point for the development of semiautomatic methodologies supporting the physician in the development of non invasive 3D diagnostic analysis over different pathologies.

5.0 Acknowledgments

6.0 Appendix

A1. Shape index and Curvedness

According to differential geometry, local surface shape is uniquely determined by the first and second fundamental forms [50]. For every $(x_0, y_0, f(x_0, y_0)) \in S$,

$$H(x_0, y_0) = \frac{(1 + f_y^2) f_{xx} - 2 f_x f_y f_{xy} + (1 + f_x^2) f_{yy}}{2(1 + f_x^2 + f_y^2)^{3/2}}, \tag{1}$$

$$K(x_0, y_0) = \frac{f_{xx} f_{yy} - f_{xy}^2}{(1 + f_x^2 + f_y^2)^2},$$

where $f_x, f_y, f_{xy}, f_{xx}, f_{yy}$ are the first and second derivatives of f in (x_0, y_0).

Gaussian and Mean curvature combine these first and second fundamental forms in two different ways to obtain scalar surface features that are invariant to rotations, translations and changes in parameterization. From equation (1), it can be derived that at any vertex v, the principal curvatures can be expressed as

$$k_i = H(v) \pm \sqrt{H^2(v) - K(v)}, \qquad i = 1, 2 \tag{2}$$

If it denote $k_1 \geq k_2$, the Shape Index $S(v)$ and the Curvedness $C(v)$ at this vertex are defined as

$$S(v) = -\frac{2}{\pi} \arctan \frac{k_1(v) + k_2(v)}{k_1(v) - k_2(v)}, \qquad S(v) \in [-1, 1], \tag{3}$$

$$C(v) = \sqrt{\frac{k_1^2(v) + k_2^2(v)}{2}} \tag{4}$$

A2. Algorithms for 3D mesh segmentation

Method	Features	Criteria	Advantage	Disadvantage
Region Growing	Variable-order approximating polynomials, mean and gaussian curvature	Distance of points from the polynomial surface, derivatives estimates of points close to the polynomial surface derivatives	- Simple to implement. - Some noise could be absorbed, when regions are still small	- The output depends on the choice of the threshold. - Over-segmentation
	Approximating polynomial surface, normals of the point cloud	Distance of points from the polynomial surface, normal orientation of points compared with the direction of the Z axis		
	Principal Curvatures	A triangle is added to a region based on the clustering of the Principal Curvatures		
	Gaussian Curvature	Gaussian Curvature value above a user defined threshold		
	Dihedral angle of adjacent triangles	Convexity validation based on the dihedral angles		
	Superquadrics	Average error-of-fit between surfaces points and Superquadric		
Watershed based	Deviation from flatness, Gaussian curvature, Mean curvature, Root mean square curvature, absolute curvature	Points belong to the catchment basins that the function f create	Affine-invariant segmentation	-Over-segmentation. - Good segmentations only for uniform meshes. - Sensitive to noise
	Minimum curvature, normal Curvature	Points belong to a catchments basin if their minimum curvature are above a threshold, additionally points are added to the segments based on their normal curvature		
	Dihedral Angles	Edges belong to the catchment basins that the function f create		
Reeb Graphs	Mean Curvature, Protrusion Function	Discrete Reeb Graph Connectivity, Average Curvature	Affine-invariant segmentation	-Determination of appropriate height functions. - Highly sensitive to noise
Model based	Electrical charge density distribution	Boundary points are selected based on the minima of the electrical charge density distribution	Less sensitive to noise	- Only trace segmentation boundaries. -Surface with concave area contained in segmentation area.
Skeleton based	Geometric and parametric function	Critical points of the geometric and parametric function define the segmentation boundaries	It is noise resistant.	Application of smoothing filters on the parametric functions
Clustering	Plane, surface normals, irregularity measure	Planarity, Orientation Bias and Compact Shape Bias	Clustering algorithms do not require training data	Clustering algorithms do require an initial segmentation
	Area and perimeter of regions, normals of surface	Area size, Boundary Smoothness, Region Flatness		

|				
	Plane, sphere and Cylinder primitives	Points are clustered based on their best fit to the plane, sphere and cylinder primitive		
	Slippable motions	The number and compatibility of slippable motions define segmentation areas		
	Geodesic distance and dihedral angles	Triangles are clustered based on a distance function defined by a weighted sum of geodesic distances and dihedral angles.		
Spectral Analysis	Eigenvalues of the affinity matrix	-Eigenvalue clustering of the affinity matrix define the labeling of the triangles into segmentation areas		This algorithm requires an initial segmentation.
Explicit Boundary Extraction	Minimum Curvature	Centricity of the contour, Salience test	It produces closed segmentation boundaries	
Critical Points based	Critical Points, Dihedral angles	Centrality of the points of the mesh		
	Critical Points, Geodesic Distance, Protrusion Function	Geodesic and Angular distances from critical points of the mesh define zones where possible segmentation boundaries belong	Less sensitive to noise	Mesh with protrusions.
Multiscale Shape Descriptors	Integral Gaussian curvature, Contours generated by the intersection of sphere with the mesh	Number of contours generated by the intersection of sphere and surface	It combines the benefits of the wavelet transform and Fourier transform	After the Fourier transform, local shape information is distributed to all coefficients and not localized in the frequency domain.
Markov Random Fields	Shape Index, Curvedness	Convexity	Robust method	Computationally very taxing.
Direct Segmentation	Normal vectors, various types of filters that distinguishes between the surfaces type	Points of the mesh are tested upon a sequence of surface hypothesis in order to determine to which type of surface they belong	stability	
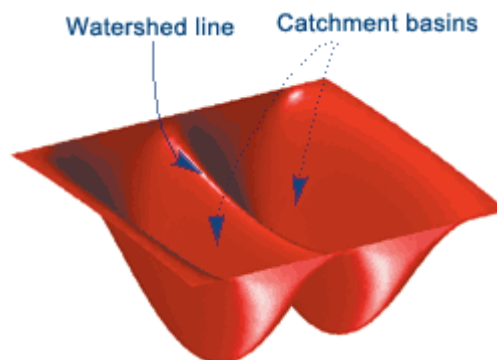
Figure A2.1. Watershed algorithm.

(a)   (b)
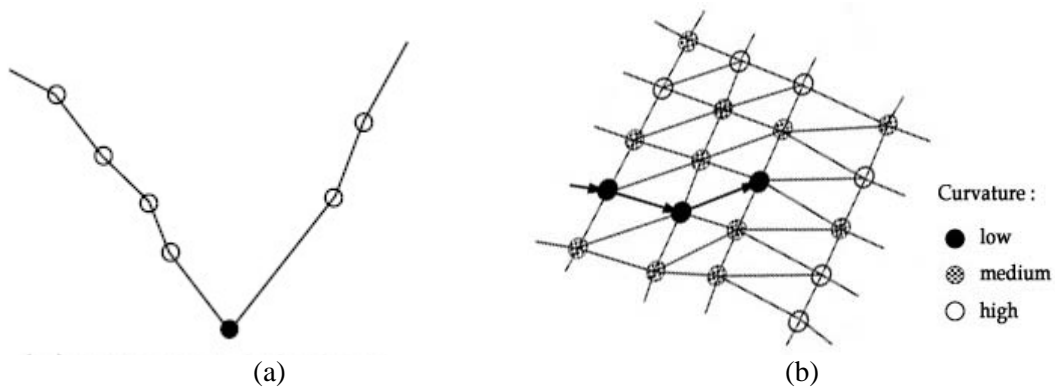
Figure A2.2. (a) Minima labelling, (b) the top-down approach on 3D mesh.

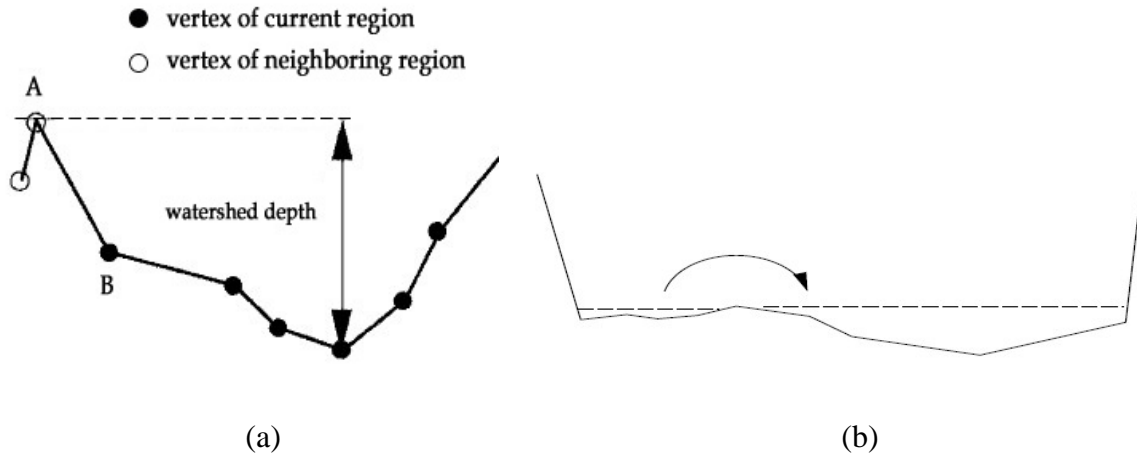(a)   (b)

Figure A2.3. (a) Watershed depth, (b) merging adjacent regions with shallow depths.

A3. Normalized Error

The Normalized Error is evaluated as the ratio between the absolute value of the difference of two states of a variable and the relevant expanded uncertainty. The expanded uncertainty U of the difference of the average values $m_{ALE} - m_M$ is given by:

$$U = t_{\alpha,v} \cdot s = t_{\alpha,v} \cdot \sqrt{s^2_{m_{ALE}} + s^2_{m_M}}$$

where $t_{\alpha,v}$ is the Student distribution variable for an acceptable risk of error α and a number of degrees of freedom v. The Normalized Error E_N is hence calculated using the formula:

$$E_N = \frac{|m_{ALE} - m_M|}{U} = \frac{|m_{ALE} - m_M|}{t_{\alpha,v} \sqrt{s^2_{m_{ALE}} + s^2_{m_M}}}$$

In the presented application, the value of the $t_{\alpha,v}$ are:
- $t_{\alpha,v,\,male} = 2.228139$ with $\alpha=0.05$ and $v=10$,
- $t_{\alpha,v,\,female} = 2.262157$ with $\alpha=0.05$ and $v=9$.

7.0 References

1. AGARWAL M. G., ANCHA C., SHAH M., PURI A., PAI S., *Limb Salvage Surgery for Osteosarcoma: Effective Low-cost Treatment.* Clinical Orthopaedics and Related Research, 459, 2007, 82-91.
2. WORZ S., ROHR K., *Localization of anatomical point landmarks in 3-D medical images by fitting 3-D parametric intensity models.* Med. Image Anal., vol. 10, no. 1, pp. 41–58, 2006.
3. LIU X., KIM W., DRERUP B., *Foot 3D characterization and localization of anatomical landmarks of the foot by FASTscan.* Real-Time Imaging 2004;10(4):217–28.
4. YAHARA H., HIGUMA N., FUKUI Y., NISHIHARA S., MOCHIMARU M., KOUCHI M., *Estimation of anatomical landmark positions from model of 3-dimensional foot by the FFD method.* Systems and Computers in Japan 2005;36(6):26–38.
5. GRIFFIN F.M., MATH K., SCUDERI G.R., INSAL J.N., POILVACHE P.L., *Anatomy of the epicondyles of the distal femur MRI analysis of normal knees.* Journal of Arthroplasty 2000;15(3):354–9.
6. VAN SINT JAN S., *Colour atlas of skeletal landmark definitions: guidelines for reproducible manual and virtual palpations.* Churchill Livingstone/Elsevier; 2007.
7. DELLA CROCE U., CAPPOZZO A., KERRIGAN D.C., *Pelvis and lower limb anatomical landmark calibration precision and its propagation to bone geometry and joint angles.* Medical and Biological Engineering and Computing 1999;37(1): 155–61.
8. YANG J., LING X., LU Y., WEI M., DING G., *Cephalometric image analysis and measurement for orthognathic surgery.* Medical and Biological Engineering and Computing 2001;39(3):279–84.
9. MAUDGIL D.D., FREE S.L., SISODIYA S.M., LEMIEUX L., WOERMANN F.G., FISH D.R., et al., *Identifying homologous anatomical landmarks on reconstructed magnetic resonance images of the human cerebral cortical surface.* Journal of Anatomy 1998;193(4):559–71.
10. COOMBES A.M., MOSS J.P., LINNEY A.D., RICHARDS R., JAMES D.R., *A mathematical method for comparison of three dimensional changes in the facial surface.* Eur J Orthod. 13:95–110; 1991.
11. YANG X., DONG Y., LONG X., ZHANG G., KAO C., *The evaluation of jaw function subsequent to bilateral sagittal split osteotomy.* Oral Surg Oral Med Oral Pathol Oral Radiol Endod 2005; 100(1):10–16.
12. HUTTON, T., *Dense Surface Models of the Human Face.* PhD thesis, University College London, 2004.
13. COLBRY D., STOCKMAN G., JAIN A., *Detection of anchor points for 3D face verification.* In *Proc.* IEEE Conf. on Computer Vision and Pattern Recognition, pages 118–125, New York, NY, Jun 2006.
14. MORENO A.B., SANCHEZ A., VELEZ J.F., DIAZ F.J., *Face recognition using 3D surface-extracted descriptors.* In Irish Machine Vision and Image Processing Conference, Coleraine, Ireland, Sept. 2003.
15. NAIR P., ZOU L., CAVALLARO A., *Facial scan change detection.* In Proc. European Workshop on the Integration of Knowledge, Semantic and Digital Media Technologies, pages 77–82, London, UK, Dec. 2005.
16. COOTES T.F., TAYLOR C.J., COOPER D.H., GRAHAM J., *Active shape models: their training and application.* Computer Vision and Image Understanding, 61(1):38–59, Jan. 1995.

17. MATTHEWS I., BAKER S., *Active appearance models revisited.* Int. Journal of Computer Vision, 60(2):135 – 164, Nov. 2004.

18. BLANZ V., VETTER T., *A morphable model for the synthesis of 3D faces.* In Proc. 26th annual conference on Computer graphics and interactive techniques, pages 187– 194, Los Angeles, CA, Aug. 1999.

19. DICKENS M.M., GLEASON S.S., SARI-SARRAF H., *Volumetric segmentation via 3D active shape models.* In Proc. IEEE Southwest Symposium on Image Analysis and Interpretation, pages 248–252, NM, 2002.

20. BUCHAILLARD S., ONG S.H., PAYAN Y., FOONG K.W.C., *Reconstruction of 3D tooth images.* In Proc. IEEE International Conference on Image Processing, pages 1077– 1080, Singapore, Oct. 2004.

21. THIRION J.P., *New feature points based on geometric invariants for 3D image registration.* Int. J. Comput. Vis. 18 (2), 121–137.(1996)

22. ROHR K., *On 3D differential operators for detecting point landmarks.* Image Vis. Comput. 15 (3), 219–233 (1997)

23. FRANTZ S., ROHR K., STIEHL H.S., *Multi-step differential approaches for the localization of 3D point landmarks in medical images.* J. Comput. Inform. Technol. 6 (4), 435–447 (1998)

24. HARTKENS T., ROHR K., STIEHL H.S., *Evaluation of 3D operators for the detection of anatomical point landmarks in MR and CT images.* Comput. Vis. Image Und. 85, 1–19 (2002)

25. BEIL W., ROHR K., Stiehl H. S., *Investigation of approaches for the localization of anatomical landmarks in 3D medical images.* In H.U. Lemke, M.W. Vannier, and K. Inamura, editors, Proc. Computer Assisted Radiology and Surgery (CAR'97), pp. 265-270, Berlin, FRG. Elsevier Science. (1997)

26. NAIR P., CAVALLARO A., *Region segmentation and feature point extraction on 3d faces using a point distribution model.* ICIP 2007.

27. MORENO A., SANCHEZ A., VELEZ J., DIAZ F., *Face recognition using 3d surface extracted descriptors.* Proceedings of the Irish Machine Vision and Image Processing 2003, 2004 (ISBN 1-85923-177-2).

28. FLYNN P.J., JAIN A.K., *On reliable curvature estimation.* In Proceedings of the IEEE Conference on Computer Vision and Pattern Recognition, pp. 110–116, 1989.

29. BESL P.J., JAIN R.C., *Invariant surface characteristics for 3D object recognition in range images.* Computer Vision, Graphics and Image Processing 33, pp. 33–80, 1986.

30. VEMURI B.C., MITICHE A., AGGARWAL J.K., *Curvature-based representation of objects from range data.* Image and Vision Computing 4, pp. 107–114, May 1986.

31. FAN T.J., MEDIONI G., NEVATIA R., *Description of surfaces from range data using curvature properties.* In Proceedings of the IEEE Conference on Computer Vision and Pattern Recognition, pp. 86–91, 1986.

32. ITTNER D.J., JAIN A.K., *3-D surface discrimination from local curvature measures.* In Proceedings of the IEEE Conference on Computer Vision and Pattern Recognition, pp. 119–123, 1985.

33. SHI J., MALIK J., *Normalized Cuts and Image Segmentation.* IEEE Transactions on Pattern Analysis and Machine Intelligence, 22(8), 2000, 888-905.

34. TANG C.K., MEDIONI G., *Robust estimation of curvature information from noisy 3d data for shape description.* In International Conference on Computer Vision, pp. 426–433, 1999.

35. TRUCCO E., FISHER R.B., *Experiments in curvature-based segmentation of range data*. IEEE Transactions on Pattern Analysis and Machine Intelligence 17(2), pp. 177–182, 1995.

36. ANGELOPOULOU E., WOLFF L., *Sign of gaussian curvature from curve orientation in photometric space*. IEEE Transaction on Pattern Analysis and Machine Intelligence 20, pp. 1056–1066, Oct 1998.

37. KOENDERINK J. J., VAN DOORN A. J., *Surface shape and curvature scales.* Image and Vision Computing, 10, 1992, 557-565.

38. HOFFMAN D., RICHARDS W., *Parts of recognition*. Cognition 18, 1984, 65–96.

39. KATZ S., TAL A., *Hierarchical Mesh Decomposition Using Fuzzy Clustering and Cuts*. ACM Trans. on Graphics, 22(3), 2003, 954-961.

40. KATZ S., LEIFMAN, G., TAL A. *Mesh Segmentation using Feature Point and Core Extraction*. The Visual Computer, 21(8-10), 2005, 649-658.

41. LEE Y., LEE S., SHAMIR A., COHEN-OR D., SEIDEL H.P., M*esh Scissoring with Minima Rule and Part Salience*. Computer-Aided Geometric Design, 22(5), 2005, 444-465.

42. LEE Y., LEE S., *Geometric snakes for triangular meshes*. Computer Graphics Forum (Eurographics 2002), 21(3), 2002, 229-238.

43. LIU R., ZHANG H., *Segmentation of 3D meshes through spectral clustering.* Pacific Conference on Computer Graphics and Applications, 2004, 298–305.

44. PAGE D. L., KOSCHAN A., ABIDI M., *Perception-based 3D triangle mesh segmentation using fast marching watersheds*. In Proc. of Computer Vision and Pattern Recognition, 2003, 27-32.

45. PAGE D. L., KOSCHAN A., ABIDI M., ZHANG Y., *Object representation using the minima rule and superquadrics for under vehicle inspection*. In Proc. of 1st IEEE Latin American Conf. on Robotics and Automation, 2003, 91-97.

46. ZHANG Y., PAIK J., KOSCHAN A., ABIDI M. A., *A simple and efficient algorithm for part decomposition of 3D triangulated models based on curvature analysis*. Proc. Intl. Conf. on Image Processing, 2002, 273-276.

47. ZHANG H., LIU R., *Mesh Segmentation via Recursive and Visually Salient Spectral Cuts, Vision, Modelling, and Visualization (VMV).* Erlangen (GERMANY), 2005, 429-436.

48. ISO/IEC Guide 43-1, *Proficiency testing by interlaboratory comparisons -- Part 1: Development and operation of proficiency testing schemes*. International Organization for Standardization, Genève (1997).

49. VEZZETTI E.; CALIGNANO F, *Soft tissue diagnosis in maxillofacial surgery: a preliminary study on three.dimensiona face geometrical features based analysis*, AESTHETIC PLASTIC SURGERY, 2009, DOI: 10.1007/s00266-009-9410-4

50. DOCARMO M., *Differential Geometry of Curves and Surfaces*. Prentice-Hall, 1976.